Photoinduced spin angular momentum transfer into an antiferromagnetic insulator

Y. Fan,[1] X. Ma,[1] F. Fang,[1] J. Zhu,[2] Q. Li,[2] T. P. Ma,[2] Y. Z. Wu,[2] Z. H. Chen,[2] H. B. Zhao,[3,*] and G. Lüpke[1,†]

[1]*Department of Applied Science, College of William & Mary, Williamsburg, VA 23187*

[2]*Department of Physics, State Key Laboratory of Surface Physics and Advanced Materials Laboratory, Fudan University, Shanghai 200433, China*

[3]*Key Laboratory of Micro and Nano Photonic Structures (Ministry of Education), Department of Optical Science and Engineering, Fudan University, Shanghai, 200433, China*

(Received 20 January 2014; revised manuscript received 11 March 2014; published 31 March 2014)

Spin angular momentum transfer into an antiferromagnetic (AFM) insulator is observed in a single-crystalline Fe/CoO/MgO(001) heterostructure by time-resolved magneto-optical Kerr effect. The transfer process is mediated by the Heisenberg exchange coupling between Fe and CoO spins. Spin angular momentum transfer to ordered AFM spins is independent of the external magnetic field and enhances the spin precession damping in Fe, which remains nearly invariant with temperature.

DOI: 10.1103/PhysRevB.89.094428 PACS number(s): 75.78.−n

The spin angular momentum transfer effect is crucial for next generation spintronic devices, including spin random access memory (RAM) [1]. To write information into spin RAM, a spin-polarized current is usually applied to transfer spin angular momentum into a ferromagnetic (FM) metallic layer. This spin-transfer-torque (STT) effect has been demonstrated to drive ultrafast spin precession, which causes the magnetization to switch when the current density exceeds a threshold value of 5×10^6 A/cm^2 in tunnel junctions [2–4]. However, the critical current density still needs to be reduced for wide applications of spin RAM with high integration density.

Alternatively, antiferromagnetic (AFM) spins can also be modulated by the STT effect [5–7]. Spin angular momentum transfer into AFM metals has been observed via modification of the exchange bias in FM/AFM systems [8–10]. The spin-polarized current creates a nonequilibrium spin density in the AFM layer, which alters the exchange field and thus generates a spin torque. Furthermore, the torque exerted on each AFM spin is weak, causing a long decay length of the STT effect, which results in the transfer of spin angular momentum deep into the AFM layer [6]. This is in contrast to FM metals where the STT effect is a near interface effect; hence, a lower current density may be required for AFM spin reversal [7].

Spin angular momentum transfer might be achieved in FM-metal/AFM-insulator heterostructure, which would lead to a pure spin current with the advantage of avoiding a heat effect [11–13]. One possible approach to generate such a transfer is to excite FM spin precession, which exerts a torque on AFM spins due to FM-AFM exchange coupling. As a result of angular momentum transfer, the FM spin precession would have larger damping, which can be observed in the time or frequency domain. However, to observe such an effect, a single-crystalline heterostructure is preferred since it would significantly reduce interface roughness to prevent magnon-magnon scattering (MMS) [14,15] which will also contribute to the damping. Recently, single-crystal Fe/CoO(001) heterostructures have been grown by molecular beam epitaxy (MBE) with the crystallographic axis Fe[100]//CoO[110] [16–18]. The large crystalline magnetic anisotropy energy of 3 meV/Co^{2+} in CoO [19,20] may suppress the nucleation of multi-AFM domains and local exchange fluctuations. The static magnetization measurements reveal that AFM spins favor a collinear coupling with Fe magnetic moments [17], which is a favorable configuration for studying the spin angular momentum transfer effect.

In this paper, we report on time-resolved magneto-optical Kerr effect (TRMOKE) measurements to investigate optically excited coherent spin precession in single-crystalline Fe/CoO heterostructure. The damping behavior in the Fe film changes abruptly at the Néel temperature (T_N) of the CoO layer and becomes independent of the applied magnetic field at low temperature. This observation is distinct from MMS or the dephasing effect and indicates that the spin angular momentum is transferred to the CoO spins via the FM-AFM Heisenberg exchange coupling.

The Fe/CoO bilayer is deposited on MgO(001) substrate by MBE at room temperature (RT). CoO layers with thicknesses of 1 nm, 2.5 nm, and 4 nm are grown by the reactive deposition of Co with oxygen [16,17] at a pressure of 2×10^{-6} Torr. [18]. A 5-nm-thick epitaxial Fe film is then deposited on top of the CoO layer [Fig. 1(a)]. The single-crystal structure of the CoO and Fe films is verified by reflection high-energy electron diffraction [18]. For comparison, a 5-nm-thick Fe film is directly grown on MgO (Fe/MgO). All of the samples are covered by a 3-nm-thick MgO protection layer.

Coherent spin precessions in the Fe films are investigated by TRMOKE [21] in a canted magnetization configuration where the magnetic field (H) is applied along Fe[110], as depicted in Fig. 1(a). An intense pump laser excites the magnetization (**M**) precession in the Fe film via fast modulation of the anisotropy fields [22–25]. The precession dynamics are recorded by the polarization change of a time-delayed probe beam [Fig. 1(b)]. The TRMOKE measurements are carried out using a Ti:sapphire amplifier laser system delivering 150 fs pulses at 800-nm wavelength with a repetition rate of 1 kHz. The pump beam is focused on the sample with a diameter of ∼0.2 mm and a pulse energy density of ∼0.28 mJ/cm^2. The probe beam has a smaller diameter of ∼0.1 mm and a pulse energy density of ∼0.05 mJ/cm^2. All measurements are performed after field cooling the sample from RT to ∼80 K.

*hbzhao@fudan.edu.cn

†luepke@wm.edu

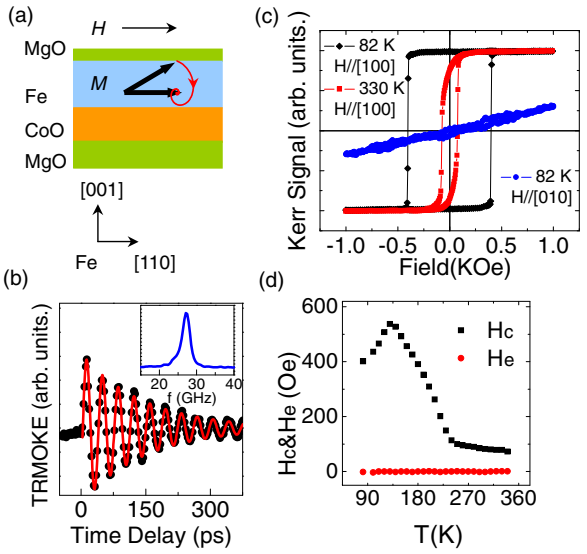

FIG. 1. (Color online) (a) Schematic presentation of magnetization (**M**) precession in Fe/CoO heterostructure with the magnetic field H applied along the Fe [110]. (b) TRMOKE data at 78 K measured with a magnetic field of $H = 600$ Oe. The solid line is a fit by the damped sine function, and the inset shows the Fourier power spectrum. (c) Longitudinal hysteresis loops for magnetic field along uniaxial easy axis [100] and hard axis [010] at 82 K and 330 K. (d) Temperature dependence of coercivity (H_c) and exchange biasing field (H_e) obtained from easy axis loops. All data are measured from Fe film grown on 2.5-nm-thick CoO (001) layer.

Longitudinal MOKE measurements indicate a negligible exchange bias (H_e) in Fe/CoO from ~80 K to above RT, as shown in Figs. 1(c) and 1(d). The absence of exchange bias is likely due to a very small number of uncompensated AFM spins at the smooth interface. However, the field cooling leads to the alignment of AFM spins along CoO ⟨110⟩ directions, which is collinear to Fe ⟨100⟩. Due to the exchange coupling of the Fe magnetization with the AFM spins, a uniaxial anisotropy appears below T_N (discussed below), and the coercivity (H_c) increases with decreasing temperature down to ~130 K, below which H_c decreases because less AFM spins are dragged to switch with FM spins [26]. As shown in Fig. 1(c), the hysteresis loop is almost square for the field along the easy axis and is much sharper at 80 K than 330 K; however, it is hard to reach saturation magnetization at the largest field, restricted by our electromagnet, along the hard axis perpendicular to the cooling field. Such results indicate a well-defined easy axis and homogeneous anisotropy of the sample.

Figure 1(b) presents TRMOKE data from a Fe film grown on a 2.5-nm-thick CoO [Fe/CoO(2.5 nm)] layer measured at 78 K with a magnetic field of $H = 600$ Oe. The data is fitted to a damped sine function, $A\exp(-t/\tau)\cos(2\pi ft)$, with precession amplitude A, time delay t, decay rate $1/\tau$, and precession frequency f. The inset shows the Fourier power spectrum, verifying the uniform precession mode of the Fe magnetization.

The spin precession dynamics in Fe/CoO(2.5 nm) is investigated as a function of the magnetic field at 78 K, 240 K, and 300 K (Fig. 2). The results are compared with TRMOKE data from Fe/MgO. The effective Gilbert damping parameter α is determined from the decay rate $1/\tau$, using [27,28]

$$\begin{aligned} \alpha &= 2/[\tau\gamma(2H\cos(\delta-\phi)+H^a+H^b)], \\ H^a &= 4\pi M_s + 2K_\perp/M_s - 2K_u\sin^2\phi/M_s \\ &\quad + K_1(2-\sin^2(2\phi))/M_s, \\ H^b &= 2K_1\cos(4\phi)/M_s + 2K_u\cos(2\phi)/M_s, \end{aligned} \tag{1}$$

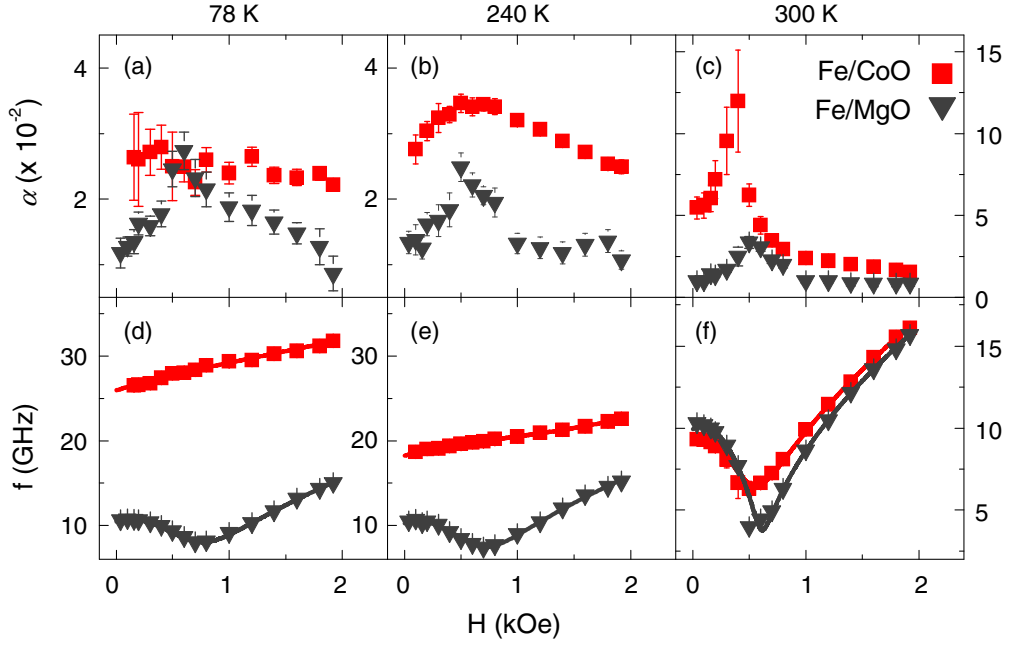

FIG. 2. (Color online) Magnetic field H dependence of (a)–(c) effective Gilbert damping α obtained from Eq. (1) and (d)–(f) precession frequency f with H applied along Fe[110] at 78 K, 240 K, and 300 K, respectively. The curves in (d)–(f) are fits of Eq. (2). The damping and frequency data obtained by TRMOKE from Fe film grown on 2.5-nm-thick CoO (001) layer and Fe/MgO are presented by ■ and ▼, respectively.

derived by solving the Landau-Lifshitz-Gilbert equation. $\gamma = \gamma_e g/2$ is the gyromagnetic ratio (for Fe, $g = 2.09$ and $\gamma_e = 1.76 \times 10^7$ Hz/Oe). δ and ϕ are the angles of H and in-plane equilibrium $\mathbf{M}$ with respect to the Fe [100] axis, M_s is the Fe-saturated magnetization, and K_u, K_1, and $K_\perp$ are the in-plane uniaxial, crystalline cubic, and out-of-plane magnetic anisotropies, respectively. K_u and K_1 have the easy axis along Fe[100], and $K_\perp$ has the easy plane of Fe(001). The values of K_u, K_1, and $K_\perp$ are determined by fitting the precession frequency f as a function of H Figs. 2(d)–2(f)], according to [27,28]

$$2\pi f = \gamma\{[H\cos(\delta-\phi)+H^a][H\cos(\delta-\phi)+H^b]\}^{1/2}. \quad (2)$$

Figure 2 compares the field dependence of the effective Gilbert damping α in Fe/CoO(2.5 nm) (■) and Fe/MgO (▼). In Fe/CoO(2.5 nm), α is nearly independent of the applied field at 78 K, and it has a weak and broad peak around 600 Oe at 240 K. We simulate the effective damping due to the dephasing caused by nonuniformity of the exchange coupling-induced anisotropy field. The results (see Appendix) indicate that the damping enhances with increasing field in the field range of 0–1920 Oe for both temperatures. In particular, the damping increases by a factor of four at 240 K. Therefore, our experimental observations rule out the dephasing processes as the dominant extrinsic damping mechanism below T_N in Fe/CoO(2.5 nm). Furthermore, we can also exclude MMS as the major damping source in our sample partially because it is induced by the local FM-AFM exchange fluctuations, as observed in polycrystalline or amorphous FM/AFM heterostructures [14,15,29–32]. Moreover, the in-plane MMS-induced damping increases with precession frequency because of the increased spin wave degeneracy [14,33,34]. However, this disagrees with the fact that the damping is invariant with H and precession frequency in single crystalline Fe/CoO(2.5 nm) at 78 K [35]. The reduced sample roughness may suppress MMS in the single-crystalline heterostructure.

In contrast, the field dependence of α in Fe/MgO (▼) at 78 K reveals a dephasing effect accompanied by the field-independent intrinsic damping. Inhomogeneities in the Fe film cause variations in the local magnetic anisotropy fields, which lead to the dephasing effect. A clear indication of this effect is that the maximum in α nearly coincides with the minimum in f, which occurs at a minimum in the effective field H_{eff} when the external field reaches a strength equal to that of the cubic anisotropy field of ~600 Oe. The weak H_{eff} leads to a large variation in the Fe spin orientation, resulting in a large dephasing effect. The dephasing effect in Fe/MgO is almost identical at 80 K, 240 K, and RT [Figs. 2(a)–2(c)]. This is in agreement with the similar anisotropy fields at different temperatures, as can be seen from the comparable precession frequencies shown in Figs. 2(d)–2(f).

The dephasing effect is nearly absent in Fe/CoO(2.5 nm) at 78 K due to the strong uniaxial magnetic anisotropy (UMA) field $2K_u/M_s$, as revealed by the enhanced precession frequency (■) shown in Fig. 2(d) [36]. This effect increases with temperature and appears at 240 K, causing a weak dependence of α (■) on H, as shown in Fig. 2(b). Since the temperature is slightly below the Néel temperature ($T_N = 255$ K) of the CoO thin film [37], the thermal energy becomes comparable to the AFM exchange energy. This causes some fluctuations in AFM spin orientation and further induces variations in FM-AFM exchange field causing the dephasing effect. At RT, the dephasing effect is dominant, and the damping exhibits a strong dependence on H, as shown in Fig. 2(c). The exchange interaction near the Fe/CoO interface forces a small fraction of CoO spins to form disordered AFM spin clusters [38], which introduce a random exchange field enhancing the dephasing effect.

From the previous discussions, we can exclude MMS and dephasing effects as the dominant damping processes in Fe/CoO(2.5 nm) below the Néel temperature. Furthermore, the CoO insulating layer eliminates the spin pumping effect [39], which can occur with a normal metal adjacent to a FM layer. The fact that α is independent of H [Fig. 2(a)] and is enhanced with respect to the intrinsic damping in Fe/MgO, as revealed at high external fields, indicates that the damping process in Fe/CoO(2.5 nm) involves both the intrinsic spin relaxation and the transfer of Fe spin angular momentum to CoO spins via FM-AFM exchange coupling and then into the lattice by spin-orbit coupling. Such a transfer process would also be independent of the external field, similar to the intrinsic damping, because the FM-AFM spin exchange stiffness, the AFM order, and the AFM spin-orbital coupling are all independent of H.

To gain further insight into the spin relaxation mechanism in Fe/CoO, we performed temperature-dependent TRMOKE measurements. Figure 3(a) reveals a sudden jump of α (▲) at T_N with $H = 1920$ Oe. Above the Néel temperature, the population of AFM spins would be very small, which limits the spin angular momentum transfer effect. Thus, the damping

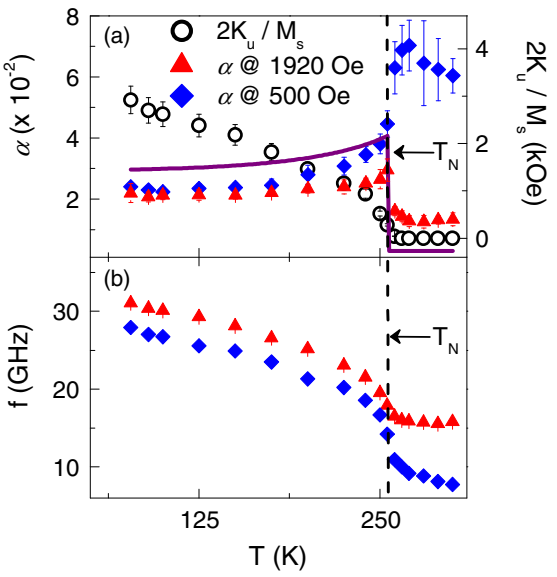

FIG. 3. (Color online) Temperature T dependence of (a) effective Gilbert damping α and UMA field $2K_u/M_s$ and (b) precession frequency of Fe film grown on 2.5-nm-thick CoO (001) layer. ▲ and ♦ present the damping data in (a) and frequency data in (b), measured using $H = 1920$ Oe and 500 Oe applied along Fe[110], respectively. o represents the UMA field. The dashed line indicates the Néel temperature T_N. The solid line is the calculated α using Eq. (4) with $\eta = 1$.

is close to the intrinsic Gilbert damping of Fe. At the Néel transition, the number of AFM spins significantly increases. The precessional Fe spins can induce precession of AFM spins via the FM-AFM coupling. This process transfers spin angular momentum into the CoO layer and thus enhances the damping of Fe spin precession.

At $H = 500$ Oe, α exhibits a large drop at T_N [Fig. 3(a)]. Above T_N, the dephasing effect caused by random exchange fields dominates as the weak H cannot align the disordered AFM spin clusters. While at T_N, the ordered AFM state nearly eliminates the dephasing effect, which causes the drop of α. As temperature decreases, the strong UMA field (o) further aligns AFM spin orientation, thus α approaches the value measured at high field. Even though the UMA field $2K_u/M_s$, calculated from the measured precession frequencies [Fig. 3(b)] using Eq. (2), strongly increases with decreasing temperature, the extracted cubic anisotropy field $2K_1/M_s$ stays nearly unchanged.

Next, we calculate the effective Gilbert damping α of Fe magnetization precession by including the FM-AFM exchange coupling in the Landau-Lifshitz-Gilbert equation,

$$d\mathbf{M}/dt = -\gamma(\mathbf{M} \times H_{\text{eff}}) + (\alpha_{\text{Fe}}/M)(\mathbf{M} \times d\mathbf{M}/dt) - (\gamma/M)(\mathbf{M} \times \mathbf{H}_{\text{FM-AFM}}) \times \mathbf{M}. \quad (3)$$

Here, $\alpha_{\text{Fe}} \approx 0.003$ is the Fe intrinsic Gilbert damping [40,41]. The last term in Eq. (3) is analogue to the STT effect [5], describing the transfer of the Fe spin angular momentum to AFM spins via FM-AFM exchange coupling, where $H_{\text{FM-AFM}} = \eta j m_{\text{Co}} e_{[100]}$ is the FM-AFM exchange field; η is the percentage of CoO AFM spins to which spin angular momentum is transferred; $j = J/(2a^2 t_{\text{Fe}} M_s \mu_B)$ is the coupling coefficient between Fe and Co magnetic moments with Fe-CoO Heisenberg exchange coefficient $J = 2.87 \times 10^{-17}$ erg [42], CoO lattice constant $a = 4.27$ Å, Fe film thickness $t_{\text{Fe}} = 5$ nm, and Bohr magneton μ_B; $m_{\text{Co}} = 3.8\mu_B$ [19] is the Co magnetic moment in CoO; and $e_{[100]}$ is the unit vector along Fe[100]. The solution of Eq. (3) yields the expression of effective Gilbert damping as

$$\alpha \approx \alpha_{\text{Fe}} + \eta j \gamma m_{\text{Co}} \cos\phi / 2\pi f, \quad (4)$$

where $\phi = 15°$–$20°$ is the angle between Fe magnetization and AFM spins determined by TRMOKE measurements. Equation (4) captures important features of α (▲) at $H = 1920$ Oe, as shown by the calculated curve (solid line) in Fig. 3(a). Above T_N, η is small, and the second term is negligible in Eq. (4), hence $\alpha \approx \alpha_{\text{Fe}}$. At the Néel transition, the AFM order is established, and the value of η cannot be neglected, which causes the jump of α at T_N. We calculate α using Eq. (4) with the above values and $\eta = 1$ below T_N. The result is shown in Fig. 3(a). We note a slight decrease of the calculated α due to the increase of precession frequency with lowering temperature. However, the measured damping is almost invariant with temperature below T_N. This small difference may be due to a varied number of rotatable and frozen AFM spins [16,43] as well as the increase of effective m_{Co} with decreasing temperature. The decrease of damping measured at $H = 500$ Oe is caused by the reduction of the dephasing effect. Here, we need to point out that the damping induced by the slow relaxer mechanism, observed in polycrystalline FM/AFM heterostructures, has strong thermal dependence due to large variation of the relaxation time of the AFM grains [44,45]. Thus, it may not account for the enhanced damping below T_N in our single-crystalline Fe/CoO sample.

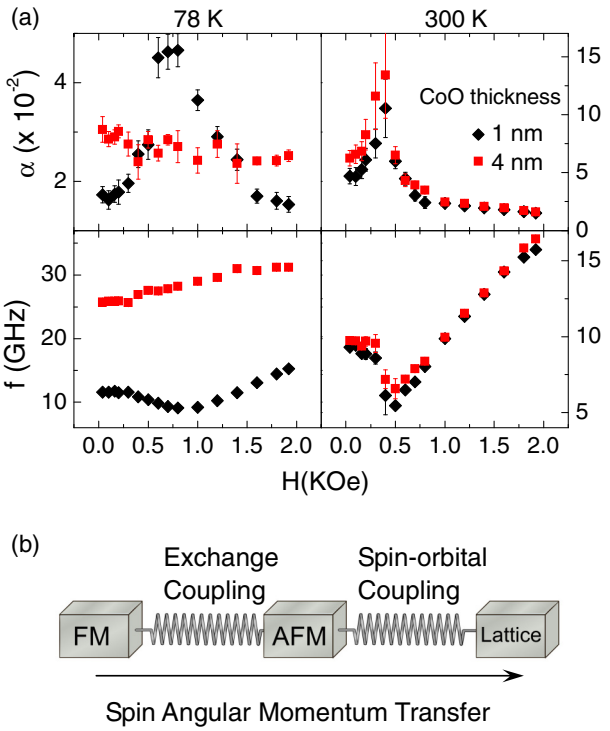

FIG. 4. (Color online) (a) Precession frequency and damping in Fe films grown on 1-nm- and 4-nm-thick CoO layer at 78 K and 300 K. (b) Schematic channel of spin angular momentum transfer from FM to AFM spins and to lattice. The exchange coupling between FM and AFM spins and the spin-orbital coupling between AFM spins and lattice are represented by springs.

We found similar damping and precession frequency for a Fe film grown on 4-nm-thick CoO, as shown in Fig. 4(a). However, for a Fe film on 1-nm-thick CoO layer, which is too thin to establish exchange torque because of the lack of AFM order, its damping and precession frequency are similar to Fe/MgO. Therefore, we can also exclude that the enhanced damping just below T_N of CoO may be caused by the presence of submonolayer FeO at the top and buried interfaces [17], although it may slightly affect the overall damping of the Fe precession. These results confirm that the uniform exchange torque exerted on the Fe magnetization by the ordered AFM spins in CoO forms the prerequisite for the observed spin angular momentum transfer.

A simple model of the spin angular momentum transfer channel in Fe/CoO is depicted in Fig. 4(b). AFM spins experience a torque from the precessional FM magnetization through FM-AFM exchange coupling (first spring). The exchange coupling has an interaction distance of ~5 nm [46], which directly transfers FM spin angular momentum to AFM bulk spins. Considering that the frozen spins in CoO may precess at frequency in the THz region because they experience very large anisotropy field, they may not be in resonance of

the FM spin precession. However, the rotatable AFM spins have much lower anisotropy energy and may be dragged by the precessing magnetization, thus offering the channel for angular momentum transfer. The transferred angular momentum of rotatable AFM spins quickly relaxes via spin-orbital coupling (second spring) to the lattice. The CoO AFM spins have a precession lifetime estimated to be ~16 ps [47], which is very short compared to the FM spin precession lifetime (~150 ps in Fe films as measured by TRMOKE), and serve as an efficient "sink" to drain spin angular momentum from the FM layer. In addition, some AFM domains with spin orientation perpendicular to the direction of the cooling field may probably be formed in CoO during the field cooling process, thus producing AFM domain walls that have resonance frequency in the GHz region. Such domain wall motion can also be a possible source to drain the angular momentum.

In conclusion, we have observed a sharp increase of the Fe spin precession damping in single-crystal Fe/CoO heterostructure just below the Néel transition temperature. The enhanced damping is field-independent and depends on the thickness of the CoO layer, which is consistent with spin angular momentum transfer into AFM insulator driven by the FM-AFM exchange coupling.

The TR-MOKE experiments, data analysis, simulations, and discussions performed at the College of William and Mary were sponsored by the DOE through Grant No. DE-FG02-04ER46127. The work at the Department of Physics, Fudan University, was supported by NSFC with Grants No. 10925416, No. 11274074, No. 91121007, and No. 11225417 and 973 projects of China (Project No. 2011CB925600). The work at the Department of Optical Science and Engineering, Fudan University, was supported by the NSFC with Grants No. 61222407 and No. 11074044 and NCET (11-0119).

APPENDIX: SIMULATION OF DEPHASING-INDUCED DAMPING BELOW T_N

In the case of magnetic disorder/dispersion (ΔK_u), the frequency broadening is given as

$$\Delta\omega_d = (|\partial\omega/\partial K_u| + |\partial\omega/\partial\phi| \cdot |\partial\phi/\partial K_u|)\Delta K_u, \quad \text{(A1)}$$

where $\partial\omega/\partial K_u = \omega(-\sin^2\phi/H^a + \cos2\phi/H^b)/M_s$, $\partial\omega/\partial\phi = \omega[(-K_1\sin4\phi/M_s - K_u\sin2\phi/M_s + H\sin(\delta-\phi)/2)/H^a - (4K_1\sin4\phi/M_s + 2K_u\sin2\phi/M_s + H\sin(\delta-\phi)/2)/H^b]$, calculated from Eqs. (1) and (2), and $\partial\phi/\partial K_u = -\sin2\phi/(2K_1\cos4\phi + 2K_u\cos2\phi + HM_s\cos(\phi-\delta))$, obtained from the relationship between the equilibrium magnetization orientation ϕ and the UMA K_u. The broadening of precession frequency, $\Delta\omega_d$, results in a dimensionless dephasing-induced damping term, $\alpha_d = \Delta\omega_d/[\gamma(2H\cos(\delta-\phi) + H^a + H^b)]$, by solving the Landau-Lifshitz-Gilbert equation. Therefore, the effective Gilbert damping is

$$\alpha_e = \alpha_0 + \Delta\omega_d/[\gamma(2H\cos(\delta-\phi) + H^a + H^b)], \quad \text{(A2)}$$

where α_0 is the intrinsic Gilbert damping constant.

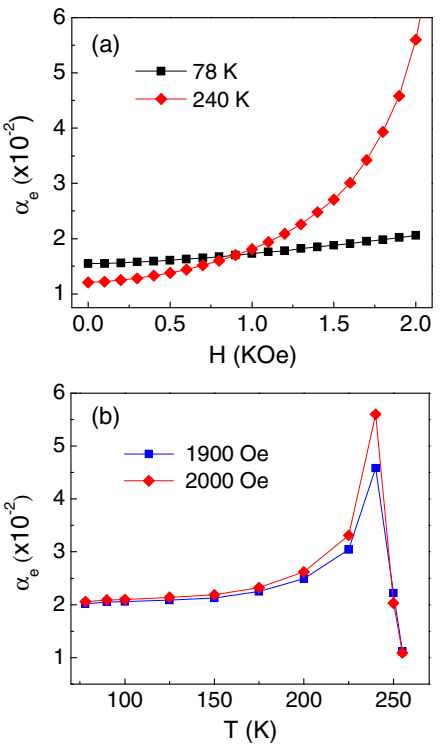

FIG. 5. (Color online) Simulation of dephasing-induced damping as a function of (a) field and (b) temperature below T_N.

Assuming a magnetic disorder below T_N, i.e., ΔK_u, which is linearly proportional to K_u, we can simulate ΔK_u-induced effective damping (dephasing). From the precession frequency, we obtain the temperature dependence of anisotropy constant K_u and K_1. By fitting the Fe/CoO(2.5 nm) damping data at 78 K with a field of 1920 Oe, we obtain ΔK_u at 78 K, and we can then calculate the field and temperature dependence of dephasing. The results of the simulation are shown in Fig. 5. The simulated results clearly show that the effective damping significantly enhances with increasing magnetic field at 240 K, and its temperature dependence exhibits a pronounced peak around 240 K for fields around 2 KOe. These simulated dephasing results are dramatically different from the measured damping, so they provide strong evidence for exclusion of inhomogeneous anisotropy-induced dephasing as the major damping source below T_N.

[1] C. Chappert, A. Fert, and F. Nguyen Van Dau, Nat. Mater. **6**, 813 (2007).
[2] M. Tsoi, A. G. M. Jansen, J. Bass, W.-C. Chiang, M. Seck, V. Tsoi, and P. Wyder, Phys. Rev. Lett. **80**, 4281 (1998).
[3] J. Grollier, V. Cros, H. Jaffrès, A. Hamzic, J. M. George, G. Faini, J. B. Youssef, H. Le Gall, and A. Fert, Phys. Rev. B **67**, 174402 (2003).
[4] C. Ralph and M. D. Stiles, J. Magn. Magn. Mater. **320**, 1190 (2008).

[5] H. V. Gomonay and V. M. Loktev, Phys. Rev. B **81**, 144427 (2010).

[6] Y. Xu, S. Wang, and Ke Xia, Phys. Rev. Lett. **100**, 226602 (2008).

[7] A. S. Núñez, R. A. Duine, P. Haney, and A. H. MacDonald, Phys. Rev. B **73**, 214426 (2006).

[8] Z. Wei, A. Sharma, A. S. Nunez, P. M. Haney, R. A. Duine, J. Bass, A. H. MacDonald, and M. Tsoi, Phys. Rev. Lett. **98**, 116603 (2007).

[9] S. Urazhdin and N. Anthony, Phys. Rev. Lett. **99**, 046602 (2007).

[10] X.-L. Tang, H.-W. Zhang, H. Su, Z.-Y. Zhong, and Y.-L. Jing, Appl. Phys. Lett. **91**, 122504 (2007).

[11] Y. Kajiwara, K. Harii, S. Takahashi, J. Ohe, K. Uchida, M. Mizuguchi, H. Umezawa, H. Kawai, K. Ando, K. Takanashi, S. Maekawa, and E. Saito, Nature **464**, 262 (2010).

[12] J. Xiao and G. E. W. Bauer, Phys. Rev. Lett. **108**, 217204 (2012).

[13] J. C. Slonczewski, Phys. Rev. B **82**, 054403 (2010).

[14] R. D. McMichael, M. D. Stiles, P. J. Chen, and W. F. Egelhoff, J. Appl. Phys. **83**, 7037 (1998).

[15] S. M. Rezende, A. Azevedo, M. A. Lucena, and F. M. de Aguiar, Phys. Rev. B **63**, 214418 (2001).

[16] J. Wu, J. S. Park, W. Kim, E. Arenholz, M. Liberati, A. Scholl, Y. Z. Wu, C. Hwang, and Z. Q. Qiu, Phys. Rev. Lett. **104**, 217204 (2010).

[17] R. Abrudan, J. Miguel, M. Bernien, C. Tieg, M. Piantek, J. Kirschner, and W. Kuch, Phys. Rev. B **77**, 014411 (2008).

[18] W. N. Cao, J. Li, G. Chen, J. Zhu, C. R. Hu, and Y. Z. Wu, Appl. Phys. Lett. **98**, 262506 (2011).

[19] V. Wagner and D. Hermann-Ronzaud, *Neutron Inelastic Scattering* (IAEA, Vienna, 1977), Part II, pp. 135–143.

[20] T. C. Schulthess and W. H. Butler, Phys. Rev. Lett. **81**, 4516 (1998).

[21] M. van Kampen, C. Jozsa, J. T. Kohlhepp, P. LeClair, L. Lagae, W. J. M. de Jonge, and B. Koopmans, Phys. Rev. Lett. **88**, 227201 (2002).

[22] Q. Zhang, A. V. Nurmikko, A. Anguelouch, G. Xiao, and A. Gupta, Phys. Rev. Lett. **89**, 177402 (2002).

[23] S. Tomimoto, M. Matsubara, T. Ogasawara, H. Okamoto, T. Kimura, and Y. Tokura, Phys. Rev. Lett. **98**, 017402 (2007).

[24] A. V. Scherbakov, A. S. Salasyuk, A. V. Akimov, X. Liu, M. Bombeck, C. Brüggemann, D. R. Yakovlev, V. F. Sapega, J. K. Furdyna, and M. Bayer, Phys. Rev. Lett. **105**, 117204 (2010).

[25] H. B. Zhao, D. Talbayev, X. Ma, Y. H. Ren, A. Venimadhav, Qi Li, and G. Lüpke, Phys. Rev. Lett. **107**, 207205 (2011).

[26] J. Zhu, Q. Li, J. X. Li, Z. Ding, C. Y. Won, and Y. Z. Wu, J. Appl. Phys. **114**, 173912 (2013).

[27] H. B. Zhao, D. Talbayev, Q. G. Yang, G. Lüpke, A. T. Hanbicki, C. H. Li, O. M. J. van't Erve, G. Kioseoglou, and B. T. Jonker, Appl. Phys. Lett. **86**, 152512 (2005).

[28] H. Suhl, Phys. Rev. **97**, 555 (1955).

[29] Bijoy K. Kuanr, R. E. Camley, and Z. Celinski, J. Appl. Phys. **93**, 7723 (2003).

[30] J. McCord, R. Kaltofen, O. G. Schmidt, and L. Schultz, Appl. Phys. Lett. **92**, 162506 (2008).

[31] G. Ju, A. V. Nurmikko, R. F. C. Farrow, R. F. Marks, M. J. Carey, and B. A. Gurney, Phys. Rev. Lett. **82**, 3705 (1999).

[32] M. C. Weber, H. Nembach, B. Hillebrands, and J. Fassbender, J. Appl. Phys. **97**, 10A701 (2005).

[33] H. Moradi and G. A. Gehring, J. Magn. Magn. Mater. **256**, 3 (2003).

[34] H. Moradi, J. Magn. Magn. Mater. **278**, 317 (2004).

[35] Moreover, the MMS can be further excluded as the dominant damping process by the temperature-dependent measurements shown in Fig. 3(a). The MMS contribution is not constant for different temperatures. Moradi and Gehring [33] and Moradi [34] demonstrated that the α due to MMS gets increased with deceasing temperature (increased resonant frequency) in similar systems but with a polycrystalline FM layer, where magnon scattering is significant, which diverges from the obtained α in Fig. 3(a).

[36] In Figs. 2(d) and 2(e), the minimum frequency in Fe/CoO occurs at zero field because of the strong uniaxial anisotropy field along Fe[100] below T_N so that Fe[110] is no longer the hard axis.

[37] The Néel temperature T_N is determined by the appearance of the UMA field [Fig. 3(a)], which is calculated from the measured precession frequencies [Fig. 3(b)] in Eq. (2). The appearance of the UMA field indicates the existence of ordered AFM spins.

[38] C. Leighton, H. Suhl, Michael J. Pechan, R. Compton, J. Nogués, and Ivan K. Schuller, J. Appl. Phys. **92**, 1483 (2002).

[39] Y. Tserkovnyak, A. Brataas, and G. E. W. Bauer, Phys. Rev. Lett. **88**, 117601 (2002).

[40] G. Woltersdorf, M. Buess, B. Heinrich, and C. H. Back, Phys. Rev. Lett. **95**, 037401 (2005).

[41] J. R. Fermin, Antonio Azevedo, F. M. de Aguiar, B. Li, and S. M. Rezende, J. Appl. Phys. **85**, 7316 (1999).

[42] K. Takano, R. H. Kodama, A. E. Berkowitz, W. Cao, and G. Thomas, Phys. Rev. Lett. **79**, 1130 (1997).

[43] J. Li, Y. Meng, J. S. Park, C. A. Jenkins, E. Arenholz, A. Scholl, A. Tan, H. Son, H. W. Zhao, C. Hwang, Y. Z. Wu, and Z. Q. Qiu, Phys. Rev. B **84**, 094447 (2011).

[44] R. D. McMichael, C. G. Lee, M. D. Stiles, F. G. Serpa, P. J. Chen, and W. F. Egelhoff Jr., J. Appl. Phys. **87**, 6406 (2000).

[45] M. Gloanec, S. Rioual, B. Lescop, R. Zuberek, R. Szymczak, P. Aleshkevych, and B. Rouvellou, Phys. Rev. B **80**, 220404(R) (2009).

[46] V. K. Valev, M. Gruyters, A. Kirilyuk, and Th. Rasing, Phys. Rev. Lett. **96**, 067206 (2006).

[47] Sóshin Chikazumi, *Physics of Ferromagnetism*, 2nd ed., edited by J. Birman, S. F. Edwards, R. Friend, C. H. Llewellyn Smith, M. Rees, D. Sherrington, and G. Veneziano (Oxford, New York, 1997), Ch. 20, Dynamic magnetization processes, pp. 572–574.